Atmos. Chem. Phys. Discuss., 10, 28151–28181, 2010
www.atmos-chem-phys-discuss.net/10/28151/2010/
doi:10.5194/acpd-10-28151-2010

Atmospheric Chemistry and Physics Discussions

A new method for retrieval of the extinction coefficient of water clouds by using the tail of the CALIOP signal

J. Li[1,2], Y. Hu[3], J. Huang[1], K. Stamnes[2], and Y. Yi[4]

[1]Key Laboratory for Semi-Arid Climate Change of the Ministry of Education College of Atmospheric Sciences, Lanzhou University, Lanzhou, 730000, China
[2]Dept. of Physics and Engineering, Stevens Institute of Tech., Hoboken, NJ, USA
[3]Climate Science Branch, NASA Langley Research Center, Hampton, VA, USA
[4]Science Systems and Applications Inc., Hampton, VA 23666, USA

Received: 9 September 2010 – Accepted: 29 October 2010 – Published: 17 November 2010

Correspondence to: Y. Hu (yongxiang.hu-1@nasa.gov)

Published by Copernicus Publications on behalf of the European Geosciences Union.

Abstract

A method is developed based on Cloud-Aerosol Lidar and Infrared Pathfinder Satellite Observations (CALIPSO) level 1 attenuated backscatter profile data for deriving the mean extinction coefficient of water droplets close to cloud top. The method is applicable to low level (cloud top < 2 km), opaque water clouds in which the lidar signal is completely attenuated beyond about 100 m of penetration into the cloud. The photo multiplier tubes (PMTs) of 532 nm detectors (parallel and perpendicular polarizations) of Cloud-Aerosol Lidar with Orthogonal Polarization (CALIOP) both exhibit a non-ideal recovery of the lidar signal after striking a strongly backscattering target (such as water cloud or surface). Therefore, the effects of any transient responses of CALIOP on the attenuated backscatter profile of the water cloud must first be removed in order to obtain a reliable (validated) attenuated backscatter profile. Then, the slope of the exponential decay of the validated water cloud attenuated backscatter profile, and the multiple scattering factor are used for deriving the mean extinction coefficient of low-level water cloud droplets close to cloud top. This novel method was evaluated and compared with the previous method by combining the cloud effective radius (3.7 µm) reported by MODIS with the lidar depolarization ratios measured by CALIPSO to estimate the mean extinction coefficient. Statistical results show that the extinction coefficients derived by the new method based on CALIOP alone agree reasonably well with those obtained in the previous study using combined CALIOP and MODIS data. Their mean absolute relative difference in extinction coefficient is about 13.4%. An important advantage of the new method is that it can be used to derive the extinction coefficient also during night time, and it is also applicable when multi-layered clouds are present. Overall, the global mean cloud water extinction coefficients during different seasons range from 26.17 to 29.46 km^{-1}, and the differences between day and night time all are small (about 1 km^{-1}). However, the global mean layer-integrated depolarization ratios of water cloud during different seasons range from 0.2 to 0.23, and the differences between day and night also are small, about 0.01.

ACPD

10, 28151–28181, 2010

1 Introduction

Low level water clouds (such as stratiform clouds within the boundary layer) are observed to occur very persistently, and to cover large areas of the globe, in particular, in the eastern parts of the subtropical ocean basins where cooler ocean currents are found. Mid-latitude anticyclones are found to exhibit more transient features (e.g. Schmetz et al., 1983). Since low level water clouds generally have high albedos, these clouds significantly decrease the amount of solar energy absorbed by the earth system, and thus reduce heating rates as compared to cloud free conditions (e.g. Randall et al., 1984; Fouquart et al., 1990; Betts and Boers, 1990). Radiation that is absorbed in a low-level water cloud layer plays an important role in the evolution of the entire cloud system. The impact of these water clouds on the radiation budget and the amount of energy that they absorb depend both upon their microphysical (such as, effective droplet radius) and macrophysical properties (such as, height, coverage) (e.g. Charlson et al., 1987; Albrecht et al., 1988; Kiehl, 1994). For example, Slingo (1990) estimated that reducing the effective diameter of stratus cloud droplet sizes from 20 to 16 µm would balance the warming due to a doubling of atmospheric CO_2. Randall et al. (1984) estimated that a 4% increase in the area of the globe that is covered by these clouds could also potentially compensate for the estimated warming due to a doubling of atmospheric CO_2. Therefore, it is very important to know the global distribution of water cloud microphysical, macrophysical and radiative properties and their relationship in order to assess their impact on climate change.

One of the most important cloud parameters related to microphysical and macrophysical properties is the optical depth τ, defined as: $\tau = \int_{z_0}^{z_1} \sigma(z)dz$, which is the vertical integration of the cloud extinction coefficient σ between the cloud boundaries z_0 and z_1. Here, the extinction coefficient σ represents the attenuation capacity of the cloud to radiation at a specific wavelength in the solar or thermal spectral range. A good knowledge of extinction coefficients in water clouds would lead to a better estimation of their impact on the surface radiative energy budget. For shortwave radiation, the

ACPD
10, 28151–28181, 2010

volume extinction coefficient σ has a very weak dependence on wavelength (Slingo and Schrecker, 1982). It is directly related to the liquid water content LWC and the equivalent droplet radius R_e as: $\sigma \approx 3\mathrm{LWC}/2R_e$, and is independent on the particle size distribution. Thus, the width of the particle size distribution has little impact on the extinction as long as the effective radius of the cloud particles does not change. For this reason methods developed for determination of cloud microstructure properties from satellite data (e.g. Arking and Childs, 1985; Nakajima and King, 1990; Han et al., 1994) have mostly been concerned with the retrieval of effective droplet radius and liquid water path. However, in this study, we focus on how to directly retrieve the extinction coefficient from satellite data without knowledge of the effective droplet radius or liquid water path.

At present, there are two approaches for inferring or retrieving the extinction coefficient of low-level water clouds: (1) derivations based on the signal measured by ground-based lidar or radar in situ measurements, and (2) inverse retrieval methods applied to combinations of passive measurements (using for example MODIS data) and power returns of active remote sensing instruments, such as space-based lidar. However, although the extinction coefficient profile (or optical depth) of a cloud can be retrieved relatively accurately from ground-based lidar or radar signals (e.g. Derr, 1980; Wang and Sassen, 2000), only one-dimensional observations are possible, and the sites are sparsely distributed, almost non-existent over the oceans. So, results from in situ measurements are commonly used to validate and evaluate satellite remote sensing retrievals (e.g. Tao et al., 2008; Mamouri et al., 2009; Kim et al., 2008; Mona et al., 2007). The advantage of remote sensing observations from instruments deployed on satellites is that high-resolution, two-dimensional distributions of the optical properties of clouds may be retrieved on a global scale. Hu et al. (2007a) derived the mean extinction coefficient of low-level water cloud tops by using collocated water cloud droplet sizes retrieved from MODIS data and CALIPSO level 2 cloud products. Nonetheless, the water cloud measurements made by active remote sensing instruments (such as, space-based lidar) are very different from those made by passive

ACPD
10, 28151–28181, 2010

remote sensing instruments (such as MODIS). Passive remote sensing of water clouds, based on measured spectral differences of reflected sunlight and thermal emissions, is used to retrieve values of optical depth for the entire vertical column. The passive sensors provide the effective droplet radius using the absorption at near infrared wavelength in the solar spectrum, and are based on the single-layer cloud assumption. So, retrievals of water cloud extinction properties based on MODIS effective radius measurements are limited to the daytime and are valid only when the single-layer cloud condition is satisfied. However, a space-based lidar (such as CALIPSO) obtains information of the cloud from the lidar signal backscattered by targets. Thus, a lidar can provide the atmospheric attenuated backscatter profile, and is not confined to daytime light conditions and a single-layer cloud structure. For these reasons, we will develop a novel method to assess the mean extinction coefficient of the low-level water cloud tops on a global scale by using space-based lidar (CALIPSO) attenuated backscatter data.

The objective of this study is to provide better knowledge of water cloud physical properties and their impact on the surface energy budget from a comparison of optical properties of water clouds between day and night. The global statistics of nighttime water cloud optical properties derived in this study is a valuable supplement to daytime retrieval results based on passive remote sensing of backscattered sunlight, and should provide a baseline for field measurements and ground based water cloud observations.

The retrieval method is introduced in Sect. 2, and described in some detail. In Sect. 3 we compare results between the new method and previous studies. Finally, a brief discussion is provided.

ACPD
10, 28151–28181, 2010

2 Methodology

Monte Carlo simulations indicate that by using layer integrated depolarization ratios and the slope of the exponential decay in the water cloud backscatter due to multiple scattering, both extinction coefficients and effective radii of water clouds can be derived from CALIPSO lidar measurements (Hu et al., 2007a). The attenuated backscatter can be expressed as:

$$\beta = \beta_0 e^{-2\eta\sigma r} \tag{1}$$

where β_0 is the peak of the attenuated backscatter, σ is the mean extinction coefficient of the low-level water cloud top, η is the multiple scattering factor, and r is the range within the water cloud. By taking the natural logarithm on both sides of Eq. (1), we have

$$\eta\sigma = \frac{\ln^{\beta} - \ln^{\beta_0}}{-2r} \tag{2}$$

Here β (the attenuated backscatter), and β_0 (the peak of attenuated backscatter) can be obtained from CALIPSO level 1 and level 2 datasets. The CALIPSO lidar probes clouds and aerosol layers to a maximum optical depth of 3 (Hu et al., 2007b), which, for dense water clouds, may correspond to a penetration depth of about 100 m, that is, near the cloud top. So, in this study, σ is the mean extinction coefficient of low-level water near cloud top, and η is the corresponding multiple scattering factor. The importance of multiple scattering of polarized light in the atmosphere has been recognized for a long time ago (e.g. Hansen, 1970a, b). For space lidars such as CALIPSO (Winker et al., 2003), which has a footprint size of 90 m at the Earths surface, water clouds can exhibit a strong depolarization signal due to the presence of multiple scattering (Hu et al., 2001). Thus, multiple scattering plays an important role in the analysis of the lidar signal. Hu et al. (2006) proposed a relationship between the integrated single scattering fraction and the accumulated linear depolarization ratio for water droplets. A simplified version of this relation is: $\eta = (\frac{1-\delta}{1+\delta})^2$ (Hu et al., 2007c),

ACPD
10, 28151–28181, 2010

where, $\delta = \int_{top}^{base} \beta_{\perp}(r)dr / \int_{top}^{base} \beta_{\parallel}(r)dr$ is the layer-integrated depolarization ratio. Cao et al. (2009) extended the idea of the accumulated depolarization for circular polarization and proposed a unique relation between the integrated single scattering fraction and the depolarization parameter, which does not depend on whether linear or circular lidar polarization is being used. This relation is independent of the measurement geometry, and the mean droplet size, and is insensitive to the width of the size distribution for most water cloud lidar returns (Hu et al., 2007a). By their studies, the multiple scattering effect of water cloud was characterized very well.

Generally speaking, if we adopt the multiple scattering relationship: $\eta = (\frac{1-\delta}{1+\delta})^2$ in Eq. (2), we can easily derive σ from the slope of the exponential decay of the water-cloud attenuated backscatter β and multiple scattering factor η (hereafter, we call it the "slope method"). However, the 532 nm photo multiplier tubes (PMTs) detectors (parallel and perpendicular) of CALIOP both exhibit a non-ideal recovery of the lidar signal after a strong backscattering target has been observed. In the absence of a strong backscattering signal, an ideal detector will return immediately to its baseline state. However, the transient response of the CALIPSO PMTs is non-ideal. Following a strong impulse signal, such as from the Earths surface or a dense water cloud, the signal initially falls off as expected but at some point begins decaying at a slower rate that is approximately exponential with respect to time (distance). In extreme cases, the non-ideal transient recovery can make it wrongly appear as if the laser signal is penetrating the surface to a depth of several hundreds of meters (e.g. McGill et al., 2007; Hunt et al., 2009). So, because of the non-ideal transient recovery, the return from strong targets will be spread by the instrument response function over several adjacent range bins, implying that the vertical distribution of the attenuated backscatter β in the water cloud will be changed. It is unlikely that the lidar receiver electronics are the source of the problem because the 1064 nm channel uses a similar design and is performing well. To demonstrate this phenomenon, Fig. 1 shows CALIPSO data images of 532 nm (top panel) and 1064 nm (bottom panel) total attenuated backscatter. The 532 nm non-ideal transient recovery is seen in the 532 nm image as a gradual transition

ACPD
10, 28151–28181, 2010

of colors from high attenuated backscatter values to lower ones for strong backscatter targets (e.g. stratus deck on the left, and the Antarctic surface return on the right). Compare these features to the 1064 nm image, where the detector response is normal, and these features appear as an almost solid band of white. For example, the right parts of 532 nm and 1064 nm images (that is, Antarctic surface) clearly illustrate that the 532 nm signal appears to continue hundreds of meters beneath the ice surface while the 1064 nm signal does not exhibit this behavior. However, it is worth notice that the cirrus cloud structure (center right) looks about the same in both the 532 nm and 1064 nm images. This is because there is little to no contribution from the transient response artifact in these weak scattering features. This effect is well documented in the literature for photon counting applications. The PMTs after-pulsing (ionization of residual gas) is the likely cause of the non-ideal transient recovery. The time scale of the effect depends on the PMTs voltage, gas species, and the PMTs internal geometry.

So, due to the non-ideal transient recovery of the CALIOP PMTs, the slope method cannot directly be used to calculate the extinction coefficient of water clouds. To retrieve a valid extinction coefficient of water clouds, we will take the following three steps:

1. First, we obtain the transient response function of CALIOP by studying CALIOP lidar signals returned from land surfaces.

2. Then, we apply an accurate de-convolution process to the lidar attenuated backscatter signal and the transient response function of CALIOP in order to remove any impacts on the attenuated backscatter profile of water cloud imparted by a non-ideal transient response of the photo-detectors.

3. Finally, after obtaining a valid attenuated backscatter profile of the water cloud by the former two steps, we can retrieve the extinction coefficient σ of water cloud from Eq. (2).

ACPD
10, 28151–28181, 2010

2.1 Transient response function of CALIOP

Prior to launch, extensive laboratory characterization of the flight detectors and their associated electronics demonstrated that the CALIPSO PMTs transient response remains the same for lidar surface returns with varing surface reflectance. This result can be independently verified using on-orbit data by studying CALIPSO's lidar signal from surfaces. It is worth notice that the strongest of the CALIPSO backscatter signals are generated by ocean and land surfaces that are covered by snow or ice (see the Antarctic surface return part of Fig. 1). In the 532 nm parallel channel, the peak signals for snow and ice surfaces under clear skies are so strong that they usually saturate the digitizers. Unlike the parallel component, the cross-polarized (perpendicular) component of the ground returns for most land and ocean surfaces are generally not saturated. As a result, in this study, only land surfaces that are not covered by snow or ice were used to assess the transient response of CALIOP at three channels. We analyze the CALIOP transient response for different land surface types using on-orbit CALIPSO Level-1 data (July 2006, October 2006, January 2007) at different regions by using a low-pass filter. We calculate the transient response function F of CALIOP:

$$F = \frac{\beta_i}{\sum_{i=p-1}^{i=p+10} \beta_i} \tag{3}$$

by using twelve adjacent lidar bins of land surface returns. The twelve range bins starting from the one range bin before the peak to the tenth range bin after the surface peak return. Here β_i is the attenuated backscatter of each bin, which is the same β as in Eqs. (1) and (2), i is the range bin number, and p is the peak surface return range bin. Hu et al. (2007d) presented a technique to provide improved lidar altimetry from CALIPSO lidar data by using the transient response of CALIOP, and verified that the tail-to-peak signal ratios are independent of the surface reflectance.

Figure 2 shows the transient response function F of CALIOP derived from the land surface return at three channels. The different colors are for different regions (surface

ACPD
10, 28151–28181, 2010

types are different) and seasons. The left, middle and right panels are for the parallel channel (P532), perpendicular channel (S532) and T532 channel (perpendicular and parallel components), respectively. It is clear that the transient response of CALIOP at different months and surface types almost are same. Although the method described in this study can be applied to both 532 nm channels (parallel and perpendicular polarization), only the results from the 532 nm parallel channel are presented in this paper.

2.2 Corrected water cloud attenuated backscatter

Actually, current water cloud attenuated backscatter signal was measured by CALIOP is a convolution result between the corrected cloud attenuated backscatter and transient response function F of CALIOP (see Eq. 4). After obtaining the transient response function of CALIOP, we may retrieve the corrected water cloud attenuated backscatter signal by using a de-convolution technique.

$$\sum_{i=1}^{n} \beta^{i}_{\text{cloud\_corrected}} \times F_{n-i+1} = \beta^{n}_{\text{cloud\_current}} \quad (n = 1,2,3,4\ldots) \tag{4}$$

Figure 3 shows the cloud attenuated backscatter signal retrieved beneath the water cloud peak return and the observed attenuated backscatter signal by CALIOP. The red line is observed (current) water cloud attenuated backscatter signal and the blue line is the retrieval (corrected or real) cloud signal. The results show that the transient response of CALIOP PMTs can affect the vertical distribution (that is, the waveform) and magnitude of the water cloud attenuated backscatter signal. After de-convolution process, the slope of the exponential decay of the water cloud attenuated backscatter, may be obtained by using a linear fit to the 3 range bins underneath the peak of the water cloud lidar return and the peak return bin itself. According to Eq. (2), the extinction coefficient of low-level water cloud top thus can be derived from the slope and multiple scattering factor of the water cloud.

ACPD
10, 28151–28181, 2010

3 Results

3.1 Comparison of extinction coefficient derived from different methods

Hu et al. (2007a) derived the mean extinction coefficient of water cloud top by combining the cloud effective radius (3.7 µm) reported by MODIS with the lidar depolarization ratios measured by CALIPSO (see Eq. 5).

$$\sigma = \left(\frac{R_e}{R_{e0}}\right)^{1/3} \left\{1 + 135\frac{\delta^2}{(1-\delta)^2}\right\} \quad (5)$$

This relation is derived from Monte Carlo simulations that incorporate the CALIPSO instrument specifications, viewing geometry, and footprint size. Here, σ is the water cloud top mean extinction coefficient, and R_e is water cloud effective droplet radius from MODIS data. R_{e0} equals 1 µm. δ is the layer-integrated depolarization ratio from CALIPSO Level 2 cloud products. The method (hereafter, we call it "Hu's method") need collocated water cloud droplet sizes retrieved from MODIS 3.7 µm data for CERES (Minnis et al., 2006). The number of photons scattered into the forward direction increases with particle size. Thus, the chance of the photon being absorbed at the near-infrared wavelengths before returning back to space increases with size. For the same optical depths, water clouds with larger droplets are darker in the near-infrared wavelengths.The effective droplet radius derived from the absorption at 3.7 µm reflects the average size information from the very top part of water clouds (Platnick, 2000), with a vertical penetration depth similar to the CALIPSO lidar signal. So, Hu's method is a simple and reliable technique for evaluating and verifying the results of the slope method during daytime.

In this study, the results of Hu's method are based on four months (January 2008, April 2008, July 2007 and October 2007) MODIS 1 km cloud data from Aqua and CALIPSO Level 2 cloud dataset. The results of the slope method are based on CALIPSO Level 1 and Level 2 data for the same months. Figure 4 shows a comparison

ACPD
10, 28151–28181, 2010

of extinction coefficients derived from the two methods. The x-axis is for slope method, and the y-axis is for Hu's method. The color values represent the sample numbers. We define the absolute relative difference as: $h = |\sigma_{\text{slope\_method}} - \sigma_{\text{Hu's\_method}}|/\sigma_{\text{Hu's\_method}}$. The mean absolute relative difference ranges from 11.4% to 15% for the four different months. The difference is largest for January 2008, reaching about 15%; and smallest for July 2007, reaching about 11.4%. Overall, the average value of the mean absolute relative differences for the four months is about 13.4%. Thus, we may conclude that the mean extinction values derived from these two methods agree well with each other.

Figure 5 shows the global distributions of low-level water cloud top extinction coefficient for different months. The left panel depicts Hu's method, and the right panel is for slope method. It is clear that the global distributions of the extinction coefficient are very similar for two methods. The larger extinction values are located along the coastal regions of the continents, such as the west coasts of South America, North America and Africa. We also found that the frequency of occurrence of water clouds is higher in these coastal regions. Because the MODIS effective radius is reliable only under single-layer cloud conditions, the results of Figs. 4 and 5 are all derived from single-layer cloud samples.

Overall, the global mean extinction coefficients derived from Hu's method are about 31.13, 32.54, 31.07, 32.31 km^{-1} for July 2007, October 2007, January 2008 and April 2008, respectively. The corresponding values derived from the slope method are 29.34, 30.34, 30.4 and 30.86 km^{-1}. Their global mean relative differences are all smaller than 7%, about 1–2 km^{-1}. Thus, it is clear that the statistical results derived from the slope method are reliable and suitable for climate applications.

3.2 Comparison of extinction coefficient at daytime and nighttime

Many studies have shown that cloud microphysical and macrophysical properties appear to have a diurnal variation (e.g. Minnis and Harrison, 1984; Fairall et al., 1990; Greenwald and Christopher, 1999). The diurnal variation in cloud properties is very important for the modulation of the time-mean energy budget of the earth-atmosphere

ACPD
10, 28151–28181, 2010

system (e.g. Bergman and Salby, 1997; Dai and Deser, 1999). However, the representation of diurnal variations of cloud properties in present climate models is relatively poor and therefore limits the predictability of cloud feedbacks in a changing climate. Accurate information on the diurnal cycles of cloud properties over land and ocean would provide a key test of many aspects of the physical parameterizations in weather and climate prediction models, such as the representation of convection, turbulence and cloud processes.

In this paper, we assessed the global information of water cloud extinction coefficient at day and nighttime by using slope method. The global statistics of nighttime water cloud optical properties derived in this study constitutes a valuable supplement to daytime retrievals from passive remote sensing that depends on reflected sunlight. They should provide a baseline for field measurements and ground based water cloud observations, a meaningful contribution to the improvement of cloud parameterizations in weather and climate prediction models.

The global distributions of water cloud extinction coefficients and depolarization ratio at daytime and nighttime in a 2° by 2° grid are shown in Figs. 6 and 7. The left panel is for daytime, and the right panel is for nighttime. There are several interesting features in Fig. 6. First, global distributions of the extinction coefficient over the ocean during daytime are very similar to those obtained during nighttime. The larger extinction values are located along the coastal regions of the continents, such as west coasts of South America, North America and Africa, where the values of the extinction coefficient may exceed 40 km^{-1}. These regions also exhibit larger effective cloud droplet number concentrations (Hu et al., 2007a), and their spatial and seasonal variations show some similarity to ocean biogeochemistry processes, and in general agree with the patterns of seasonal and temporal variation in DMS concentrations in the middle and low latitudes, generated from the POP Ocean GCM by Chu et al. (2004). Second, there are more low level water clouds over land during daytime than during nighttime. We can see that water clouds are present primarily over North of South America and over the European continents during nighttime. There is a small abundance of water

ACPD
10, 28151–28181, 2010

cloud over other continents, and the extinction coefficient is lower over South America. During daytime, there are more low-level water clouds over land, such as over middle and north of Africa, the eastern and western coasts of the US continent, and the eastern coast of China. Most water clouds have higher extinction value (>40 km^{-1}) over land except north of Africa in July (<20 km^{-1}). Third, global distributions of the water cloud depolarization ratio are similar to that of the extinction coefficient. Larger depolarization ratios correspond to higher extinction values, while smaller depolarization ratios correspond to lower extinction values (Hu et al., 2007a). Table 1 lists the global mean values of the extinction coefficient, the multiple scattering factor, and the slope of exponential decay of low-level water clouds derived from the slope method. It is worth noticing that the global mean values of the extinction coefficient during daytime in Table 1 are slightly different from the results presented in Sect. 3.1. As stated in Sect. 3.1, because the MODIS effective radius is reliable only under single-layer cloud conditions, the results of Figs. 4 and 5 are all derived from single-layer cloud samples. However, because the slope method is not confined to daytime light conditions and single-layer cloud vertical structure, multi-layered cloud samples are also included in this section. Thus, the number of samples considered in Sect. 3.2 is about three times the number of samples in Sect. 3.1. In view of statistics, the results in Table 1 are more reasonable and are expected to reflect the mean conditions of low-level water cloud.

Overall, the differences in extinction coefficient, multiple scattering factor, and the slope of exponential decay of low-level water clouds between day and night are small. The global mean extinction coefficients for different seasons range from 26.17 to 29.46 km^{-1}, and the differences between day and night are all positive and about 1 km^{-1}. However, the global mean multiple scattering factor of water clouds for different seasons range from 0.41 to 0.45, and differences between day and night are small, about −0.015. The corresponding global mean depolarization ratio of low level water clouds ranges from 0.2 to 0.23, and the differences between day and night also are small, about 0.01. Here, it is worth noticing that all results above are for low-level (cloud top < 2km), nontransparent water clouds. To investigate if the differences

ACPD
10, 28151–28181, 2010

in depolarization ratio between day and night are small for water clouds at all levels, we also examined the statistics of the global mean depolarization ratio for all level water cloud (with cloud top < 6 km). The results, shown in Fig. 8, indicate that the global mean depolarization differences still are small (ranging from 0.009 to 0.019). Sassen et al. (2009) showed that the depolarization in tropospheric ice clouds tends to increase with increasing height/decreasing temperature, as expected from various ground-based lidar studies. We found that the depolarization ratio is height-dependent also in water clouds. As shown in Fig. 8, it appears to decrease with increasing height/decreasing temperature based on the global mean. The reason is unclear, and further research is needed to find out why.

4 Conclusions and discussion

In this study, a method based on CALIPSO level 1 attenuated backscatter profile was developed to derive the mean extinction coefficient of low-level water cloud droplets close to cloud top (cloud top < 2 km). Because the photo multiplier tubes (PMTs) of the 532 nm detectors of CALIOP both exhibit a non-ideal recovery of the lidar signal after it strikes a "strongly" backscattering target (such as, water cloud or surface), in the slope method presented here, we first removed effects caused by the transient response of CALIOP on the attenuated backscatter profile of water cloud in order to obtain a validated attenuated backscatter profile. Then we used the slope of the exponential decay of the validated water cloud attenuated backscatter profile, and the multiple scattering factor to derive the mean extinction coefficient of low-level water cloud top. The novel method was evaluated and compared with the previous method developed by Hu et al. (2007a) – that is Hu's method. From the analysis of CALIPSO level 1 attenuated backscatter profiles, we arrived at the following conclusions based on using the slope method:

ACPD
10, 28151–28181, 2010

1. The extinction values derived from the new method agree well with those derived from Hu's method. Their mean absolute relative difference is about 13.4%. Their global mean relative differences are all smaller than 7%, or about 1–2 km^{-1}. Because the slope method is not confined to daytime light conditions and a single-layer cloud structure, the global statistics of water cloud optical properties derived from this study is a good supplement to results retrieved from passive remote sensing, which depend on backscattered sunlight, and should provide a baseline for field measurements and ground-based water cloud observations. Thus, the slope method provides a meaningful contribution that can be used to improve cloud parameterizations in weather and climate prediction models.

2. The global distributions of the extinction coefficient of low-level water cloud tops retrieved during daytime are very similar to those retrieved during nighttime, particularly over the ocean. The global mean extinction coefficients at different seasons range from 26.17 to 29.46 km^{-1}, and the differences between day and night are all positive and just 1 km^{-1}.

3. The seasonal variation in global mean multiple scattering factor of water clouds ranges from 0.41 to 0.45, and differences between day and night are small, about −0.015. The corresponding global mean depolarization ratio of low-level water clouds ranges from 0.2 to 0.23, and the differences between day and night also are small, about 0.01.

4. The above three conclusions are all for low-level, opaque water clouds. For all-level water clouds (cloud top < 6 km), we found that the differences in the global mean depolarization ratio between day and night remain are small, ranging from 0.009 to 0.019. Moreover, the global mean depolarization decreases with increasing height/decreasing temperature, which is an unexpected finding. The reason is being investigated.

In addition, Sassen et al. (2009) showed that there are significant (about 0.11) average depolarization differences of ice clouds between day and night, which are inconsistent

ACPD
10, 28151–28181, 2010

with earlier ground-based data. The significant difference indicates the presence of artifacts in the data set related to the effects of background signals from scattered sunlight in the green laser channel; the gain selection may be one of the reasons. To investigate if the differences in the depolarization ratio between day and night are related to the gain selection, background noise or other factors, we chose different targets (such as water cloud, ice cloud, common aerosol and dust) to analyze their depolarization difference between day and night. Preliminary results indicate that the depolarization differences of spherical particles (water cloud or common aerosols, such as clean continental aerosol) are small (<0.02). Larger differences (>0.04) are found for non-spherical particles (ice clouds or dust). Moreover, the depolarization ratios of targets may be more reliable after April 2007 (improved data quality). So, we conclude that the larger depolarization differences of ice cloud or dust may be real, and perhaps related to the cloud dynamics. However, these are just preliminary results, and further research is needed to better understand the diurnal differences in the CALIPSO depolarization values.

Many studies had shown that aerosols (such as, dust and smoke) have important impact on the variation of cloud properties (such as, effective droplet radius, number concentration and radiation forcing) (e.g. DeMott et al., 2003; Huang et al., 2006a, b; Su et al., 2008). In this study, the effect of aerosol to cloud was not considered. That is, the slope of the exponential decay of the validated water cloud attenuated backscatter profile may bear a little variation due to the aerosol loading, particularly over the western coast of Africa (smoke is abundant due to frequent burning activities). Hence, more studies about the interaction between aerosol and clouds over these regions (higher aerosol optical depth) would be needed in the future.

Generally speaking, the effective droplet radius and effective number concentration of water clouds can be directly derived from Eq. (5) when the mean extinction coefficient σ was retrieved from CALIPSO level 1 data by the slope method. However, the errors in the extinction coefficient will be magnified when σ is subsequently used to derive the effective radius, particularly when the extinction coefficient is small, such

ACPD
10, 28151–28181, 2010

as over the ocean. Therefore, the slope method is inadequate for accurate retrieval of the effective droplet radius of water cloud at present. Nonetheless, primary results (not shown in this paper) of droplet radii retrieved by the slope method show that the effective radius is lower over land than over ocean. The main reason may that the abundance of aerosols, leading to the formation of cloud condensation nuclei, is larger over land than ocean, so that an increase in the number density of cloud droplets tends to reduce the mean droplet radius (Twomey, 1991). This conclusion is consistent with that of Peng (2002). However, an accurate retrieval of the effective radius of water cloud droplets, especially effective number concentration by the slope method still needs more development and verification by comparisons with MODIS or ground-based Radar data.

Acknowledgements. This work is supported by the NASA radiation science program and CALIPSO project. In addition, this work is also supported by the National Science Foundation of China under Grant No. 40725015 and 40633017. Here, the authors want to also thank Hal Maring and David Considine of NASA Headquarters for the discussions and support.

References

Albrecht, B. A., Randall, D. A., and Nicholls, S.: Observations of marine stratocumulus clouds during FIRE, B. Am. Meteor. Soc., 69, 618–626, 1988.

Arking, A. and Childs, J. D.: Retrieval of clouds cover parameters from multispectral satellite images, J. Appl. Meteorol., 24, 323–333, 1985.

Bergman, J. W. and Salby, M. L.: The role of cloud diurnal variations in the time-mean energy budget, J. Climate, 10, 1114–1124, 1997.

Betts, A. K. and Boers, R.: A cloudiness transition in a marine boundary layer, J. Atmos. Sci., 47, 1480–1497, 1990.

Cao, X., Roy, G., Roy, N., and Bernier, R.: Comparison of the relationships between lidar integrated backscattered light and accumulated depolarization ratios forlinear and circular polarization for water droplets, fog-oil and dust, Appl. Opt., 48, 4130–4141, 2009.

ACPD

10, 28151–28181, 2010

Charlson, R. J., Lovelock, J. E., Andreae, M. O., and Warren, S. G.: Oceanic phytoplankton, atmospheric sulphur, cloud albedo and climate, Nature, 326, 655–661, 1987.
Chu, S., Elliott, S., and Maltrud, M.: Ecodynamic and Eddy-Admitting Dimethyl Sulfide Simulations in a Global Ocean Biogeochemistry/Circulation Model, Earth Interact., 8(11), 1–25, doi:10.1175/1087-3562, 2004.
Dai, A. and Deser, C.: Diurnal and semidiurnal variations in global surface wind and divergence fields, J. Geophys. Res., 104, 31109–31126, 1999.
DeMott, P. J., Sassen, K., Poellot, M. R., Baumgardner, D., Rogers, D. C., Brooks, S. D., Prenni, A. J., and Kreidenweis, S. M.: African dust aerosols as atmospheric ice nuclei, Geophys. Res. Lett., 30(14), 1732, doi:10.1029/2003GL017410, 2003.
Derr, V. E.: Estimation of the extinction coefficient of clouds from multiwavelength lidar backscatter measurements, Appl. Opt., 19, 2310–2314, 1980.
Fairall, C. W., Hare, J. E., and Snider, J. B.: An eight-month sample of marine stratocumulus cloud fraction, albedo, and integrated liquid water, J. Climate, 3, 847–863, 1990.
Fouquart, Y., Buriez, J. C., and Herman, M.: The influence of clouds on radiation: A climate modeling perspective, Rev. Geophys., 28, 145–166, 1990.
Greenwald, T. J., Christopher, S. A., and Chou, J.: Cloud liquid water path comparisons from passive microwave and solar reflectance satellite measurements: Assessment of sub-field of view cloud effects in microwave retrievals, J. Geophys. Res., 102(D16), 19585–19596, 1997.
Han, Q., Rossow, W. B., and Lacis, A. A.: Near global survey of effective droplet radii in liquid water clouds using ISCCP data, J. Climate, 7, 465–497, 1994.
Hansen, J. E.: Multiple scattering of polarized light in planetary atmospheres: Part I. The doubling Method, J. Atmos. Sci., 28, 120–125, 1971a.
Hansen, J. E.: Multiple scattering of polarized light in planetary atmospheres: Part II. Sunlight reflected by terrestrial water clouds, J. Atmos. Sci., 28, 1400–1426, 1971b.
Hu, Y., Winker, D. M., Yang, P., et al.: Identification of cloud phase from PICASSO-CENA lidar depolarization: A multiple scattering sensitivity study, J. Quant. Spectrosc. Radiat. Trans., 70, 569–579, 2001.
Hu, Y., Liu, Z., Winker, D., Vaughan, M., Noel, V., Bissonnette, L., Roy, G., and McGill, M.: A simple relation between lidar multiple scattering and depolarization for water clouds, Opt. Lett., 31, 1809–1811, 2006.
Hu, Y., Vaughan, M., McClain, C., Behrenfeld, M., Maring, H., Anderson, D., Sun-Mack, S.,

ACPD
10, 28151–28181, 2010

Flittner, D., Huang, J., Wielicki, B., Minnis, P., Weimer, C., Trepte, C., and Kuehn, R.: Global statistics of liquid water content and effective number concentration of water clouds over ocean derived from combined CALIPSO and MODIS measurements, Atmos. Chem. Phys., 7, 3353–3359, doi:10.5194/acp-7-3353-2007, 2007a.

Hu, Y., Vaughan, M., Liu, Z., Powell, K., and Rodier, S.: Retrieving Optical Depths and Lidar Ratios for Transparent Layers Above Opaque Water Clouds From CALIPSO Lidar Measurements, IEEE Trans. Geosci. Remote Sens. Lett., 4, 523–526, 2007b.

Hu, Y., Vaughan, M., Liu, Z., Lin, B., Yang, P., Flittner, D., Hunt, W., Kuehn, R., Huang, J., Wu, D., Rodier, S., Powell, K., Trepte, C., and Winker, D.: The depolarization-attenuated backscatter relation: CALIPSO lidar measurements vs. theory, Opt. Express, 15, 5327–5332, 2007c.

Hu, Y., Powell, K., Vaughan, M., et al.: Elevation-In-Tail (EIT) technique for laser altimetry, Opt. Express, 15, 14504–14515, 2007d.

Huang, J., Minnis, P., Lin, B., Wang, T., Yi, Y., Hu, Y., Sun-Mack, S., and Ayers, K.: Possible influences of Asian dust aerosols on cloud properties and radiative forcing observed from MODIS and CERES, Geophys. Res. Lett., 33, L06824, doi:10.1029/2005GL024724, 2006a.

Huang, J., Lin, B., Minnis, P., Wang, T., Wang, X., Hu, Y., Yi, Y., and Ayers, J. R.: Satellite-based assessment of possible dust aerosols semi-direct effect on cloud water path over East Asia, Geophys. Res. Lett., 33, L19802, doi:10.1029/2006GL026561, 2006b.

Hunt, W. H., Winker, D. M., Vaughan, M. A., Powell, K. A., Lucker, P. L., and Weimer, C.: CALIPSO lidar description and performance assessment, J. Atmos. Oceanic Technol., 26, 1214–1228, 2009.

Kiehl, J. T.: Sensitivity of a GCM climate simulation to differences in continental versus maritime cloud drop size, J. Geophys. Res., 99(23), 107–123, 1994.

Kim, S.-W., Berthier, S., Raut, J.-C., Chazette, P., Dulac, F., and Yoon, S.-C.: Validation of aerosol and cloud layer structures from the space-borne lidar CALIOP using a ground-based lidar in Seoul, Korea, Atmos. Chem. Phys., 8, 3705–3720, doi:10.5194/acp-8-3705-2008, 2008.

Mamouri, R. E., Amiridis, V., Papayannis, A., Giannakaki, E., Tsaknakis, G., and Balis, D. S.: Validation of CALIPSO space-borne-derived attenuated backscatter coefficient profiles using a ground-based lidar in Athens, Greece, Atmos. Meas. Tech., 2, 513–522, doi:10.5194/amt-2-513-2009, 2009.

McGill, M. J., Vaughan, M., Trepte, C. R., et al.: Airborne validation of spatial properties measured by the CALIPSO lidar, J. Geophys. Res., 112, D20201, doi:10.1029/2007JD008768,

ACPD
10, 28151–28181, 2010

2007.
Minnis, P. and Harrison, E.: Diurnal Variability of Regional Cloud and Clear-Sky Radiative Parameters Derived from GOES Data, Part II: November 1978 Cloud Distributions, J. Appl. Meteor., 23, 1012–1031, 1984.
Minnis, P., Geier, E., Wielicki, B., et al.: Overview of CERES cloud properties from VIRS and MODIS, Proc. AMS 12th Conf. Atmos. Radiation, Madison, WI, July 10–14, CD-ROM, J2.3., 2006.
Mona, L., Amodeo, A., D'Amico, G., and Pappalardo, G.: First comparisons between CNR-IMAA multi-wavelength Raman lidar measurements and CALIPSO measurements, Proc. SPIE, 6750, 675010, doi:10.1117/12.738011, 2007.
Nakajima, T. adnd King, M. D.: Determination of the optical thickness and effective particle radius of clouds from reflected solar radiation measurement, Part 1. Theory, J. Atmos. Sci., 47, 1878–1893, 1990.
Peng, Y. R., Lohmann, U., Leaitch, R., and Banic, C.: The cloud albedo-cloud droplet effective radius relationship for clean and polluted clouds from RACE and FIRE.ACE, J. Geophys. Res., 107(D11), 4106, doi:10.1029/2000JD000281, 2002.
Platnick, S.: Vertical photon transport in cloud remote sensing problems, J. Geophys. Res., 105(22), 919–935, 2000.
Randall, D. A., Coakley Jr., J. A., Fairall, C. W., Kropfli, R. A., and Lenschow, D. H.: Outlook for research on subtropical marine stratiform clouds, B. Am. Meteor. Soc., 65, 1290–1301, 1984.
Sassen, K. and Zhu, J.: A global survey of CALIPSO linear depolarization ratios in ice clouds: Initial findings, J. Geophys. Res., 114, D00H07, doi:10.1029/2009JD012279, 2009.
Slingo, A. and Schrecker, H. M.: On the shortwave radiative properties of stratiform water clouds, Q. J. Roy. Meteor. Soc., 108, 407–426, 1982.
Slingo, A.: Sensitivity of the Earths radiation budget to changes in low clouds, Nature, 343, 49–51, 1990.
Jing Su, Jianping Huang, Qiang Fu, Minnis, P., Jinming Ge, and Jianrong Bi: Estimation of Asian dust aerosol effect on cloud radiation forcing using Fu-Liou radiative model and CERES measurements, Atmos. Chem. Phys., 8, 2763–2771, doi:10.5194/acp-8-2763-2008, 2008.
Tao, Z., Mccormick, M. P., and Wu, D.: A comparison method for spaceborne and ground-based lidar and its application to the CALIPSO lidar, Apply Phys. B, 91, 639–644, 2008.

ACPD
10, 28151–28181, 2010

Twomey, S. A.: Aerosol, clouds and radiation, Atmos. Environ., Part A, 25, 2435–2442, 1991.
Wang, Z. and Sassen, K.: Cloud type and property retrieval using multiple remote sensors, J. Appl. Meteor., 40, 1665–1682, 2001.
Winker, D. M., Pelon, J. R., and McCormick, M. P.: The CALIPSO mission: Spaceborne lidar for observation of aerosols and clouds, Proc. SPIE, 4893, 1–11, doi:10.1117/12.466539, 2003.

ACPD
10, 28151–28181, 2010

Table 1. The averaged extinction coefficient, eta (multiple-scattering factor) and slope (extinction coefficient * eta) of low level water cloud from slope method.

Para.	Januar 2008	April 2008	July 2007	October 2007
Extinction coefficient(km^{-1})				
Day-time	29.13	29.46	27.38	28.72
Night-time	28.43	28.37	26.17	28.03
difference	0.7	1.09	1.21	0.69
Multiple scattering factor				
Day-time	0.411	0.41	0.426	0.41
Night-time	0.426	0.43	0.448	0.42
difference	−0.015	−0.02	−0.022	−0.01
Slope(km^{-1})				
Day-time	11.34	11.32	10.61	10.84
Night-time	11.45	11.58	10.62	10.98
difference	−0.11	−0.26	−0.01	−0.14
Depolarization ratio				
Day-time	0.22	0.225	0.215	0.224
Night-time	0.21	0.212	0.203	0.217
difference	0.01	0.013	0.012	0.007

ACPD
10, 28151–28181, 2010

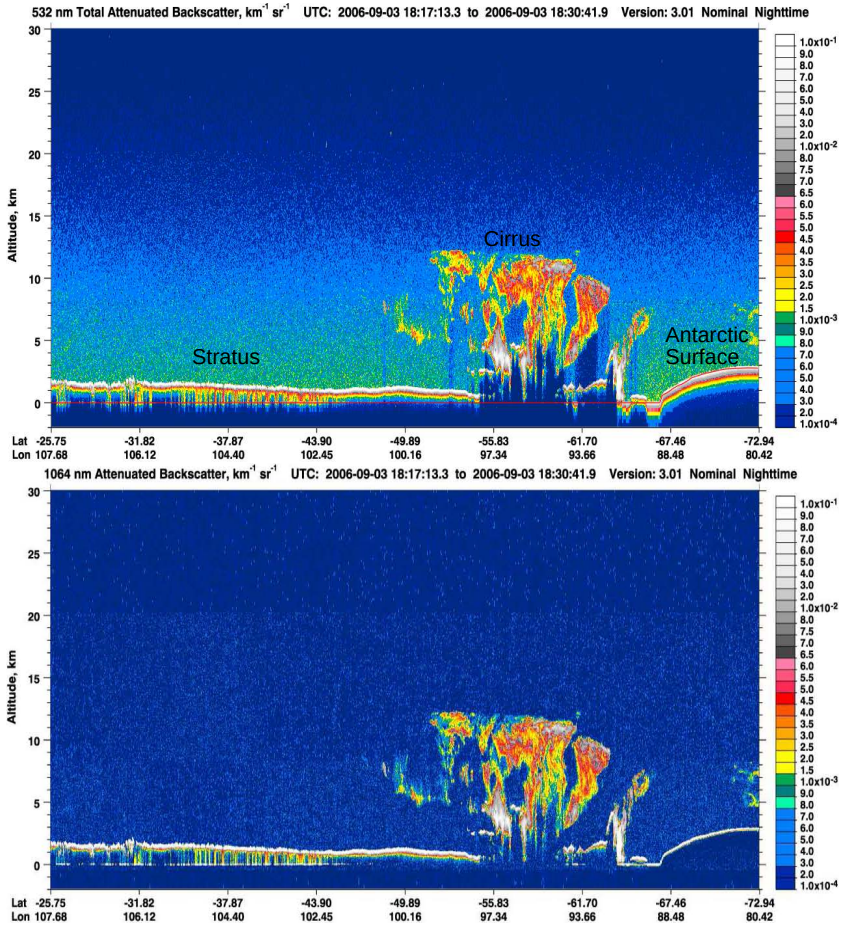

Fig. 1. CALIPSO data images of 532 nm (top panel) and 1064 nm (bottom panel) total attenuated backscatter.

ACPD
10, 28151–28181, 2010

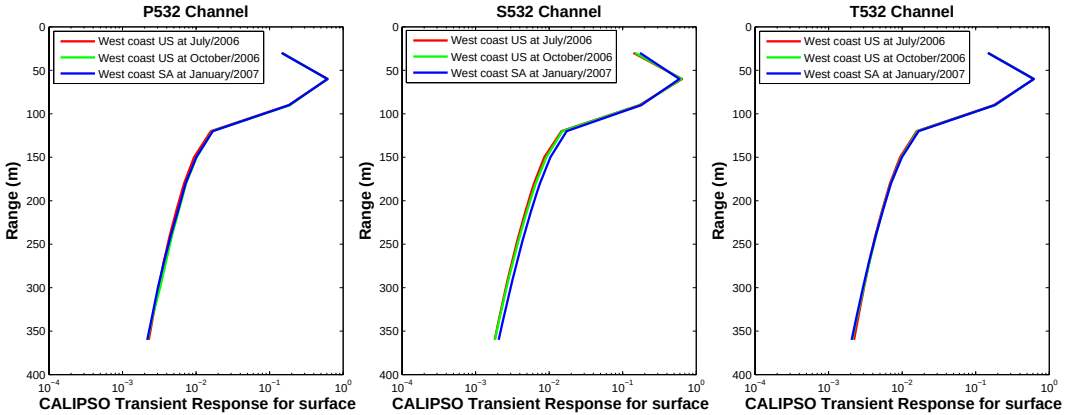

Fig. 2. Transient response of CALIOP derived from the land surface return at different months and different regions for three channels.

ACPD
10, 28151–28181, 2010

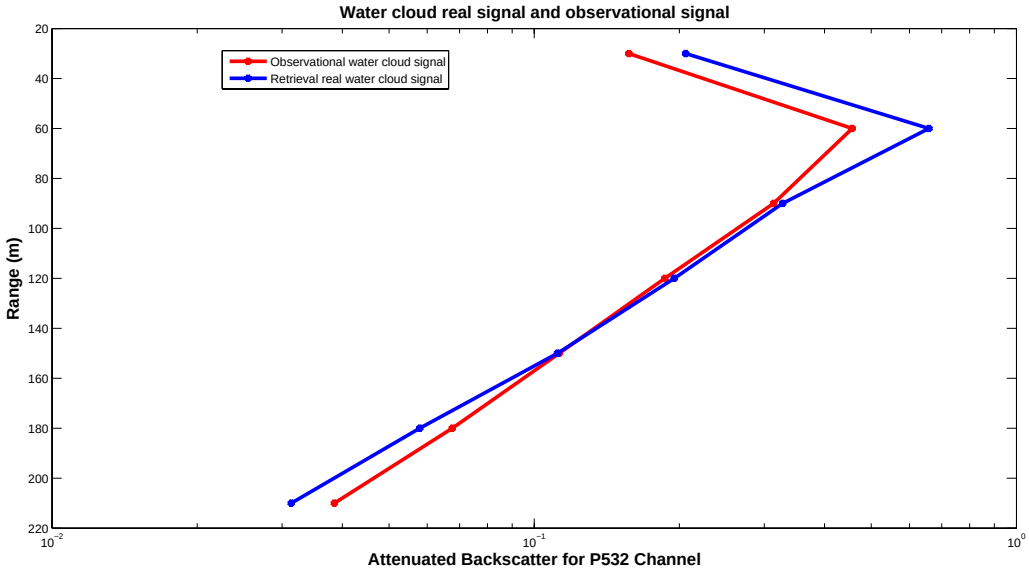

Fig. 3. The retrieved attenuated backscatter signal beneath the water cloud peak return and the observed attenuated backscatter by CALIOP. The red line is the observed (current) water cloud signal and the blue line is the retrieved (corrected or real) cloud signal.

ACPD
10, 28151–28181, 2010

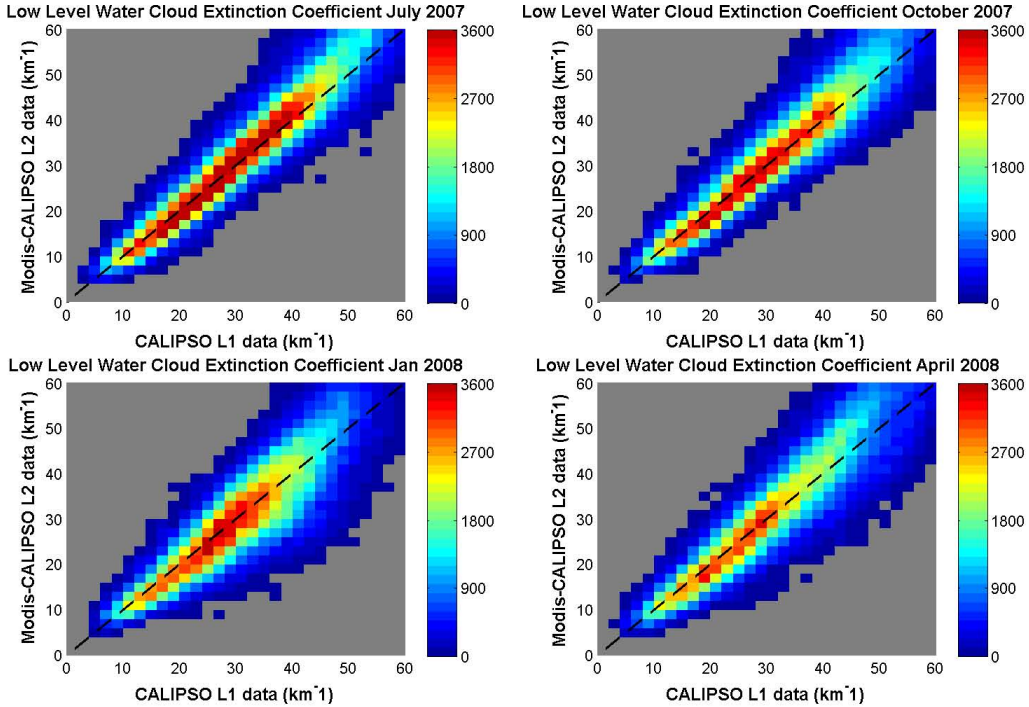

Fig. 4. Comparison of water cloud top mean extinction coefficient by using slope method and Hu's method .The x-axis is for slope method, y-axis is for Hu's method.

ACPD
10, 28151–28181, 2010

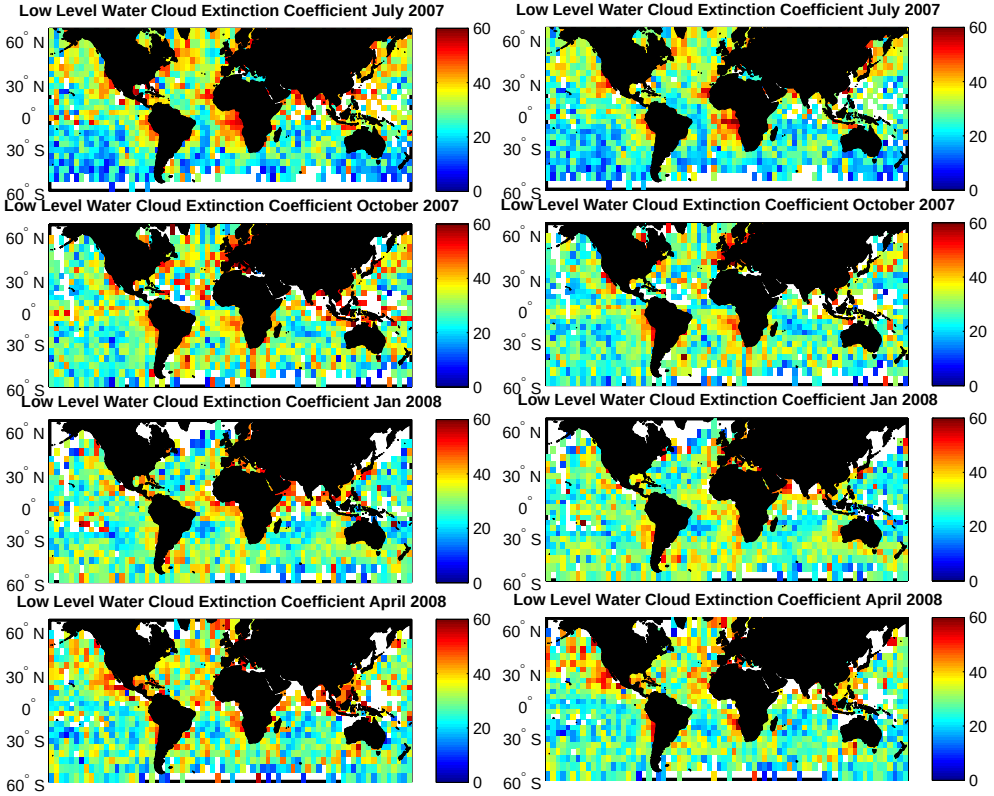

Fig. 5. The global distribution of Low level water cloud mean extinction coefficient at different months derived from the slope method (right) and Hu's method (left).

ACPD
10, 28151–28181, 2010

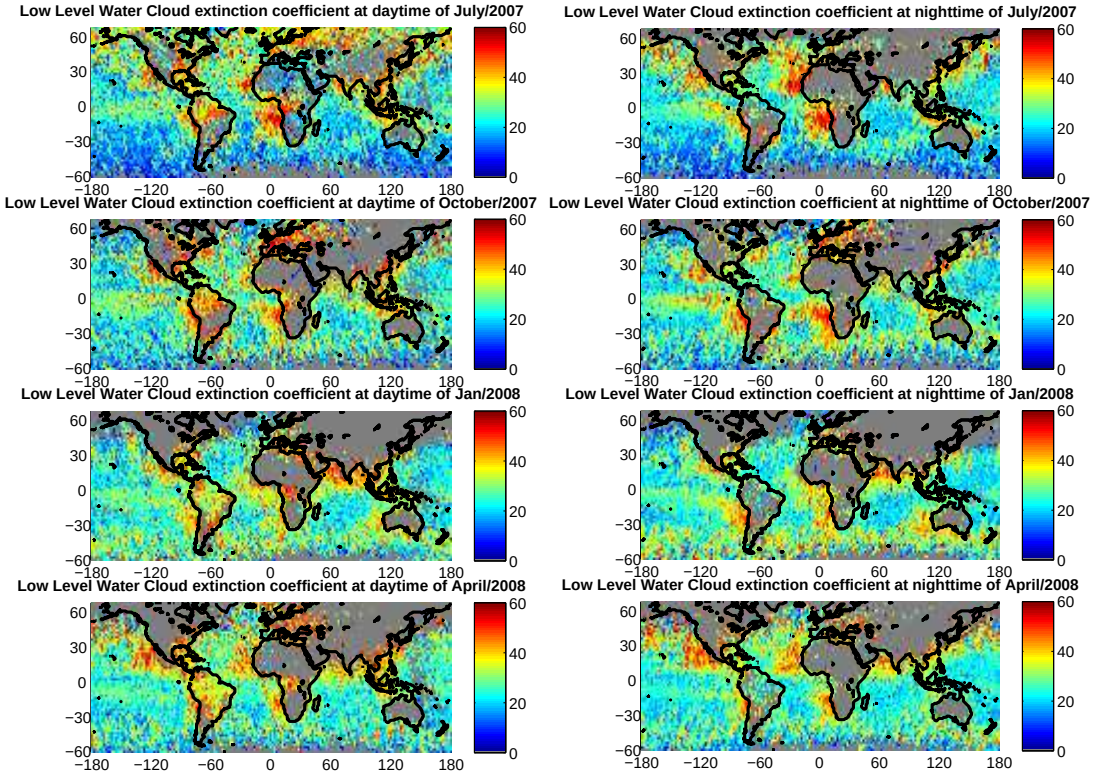

Fig. 6. The global distribution (2° by 2°) of Low level water cloud mean extinction coefficient at different months derived from the slope method at day (left) and night(right).

ACPD
10, 28151–28181, 2010

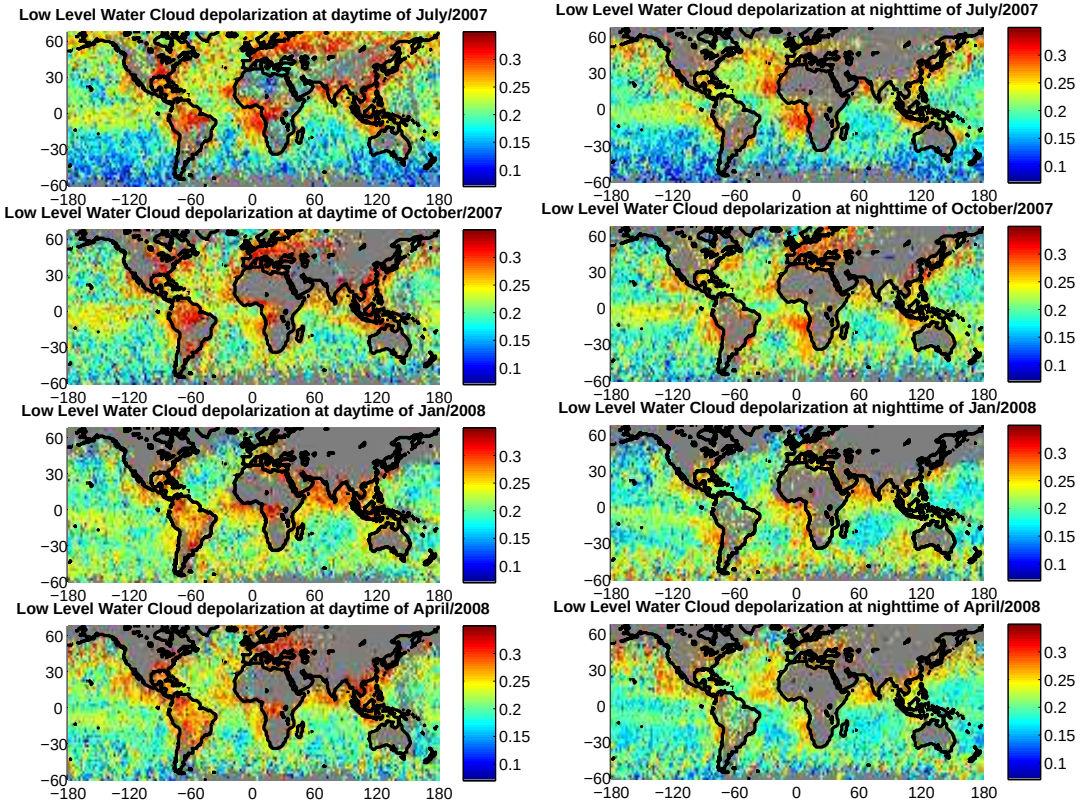

Fig. 7. The global distribution (2° by 2°) of Low level water cloud depolarization ratio at different months CALIPSO level 2 333 m cloud products. The left panel is for daytime; the right panel is for nighttime.

ACPD
10, 28151–28181, 2010

A new method for retrieval of the extinction coefficient of water clouds

J. Li et al.

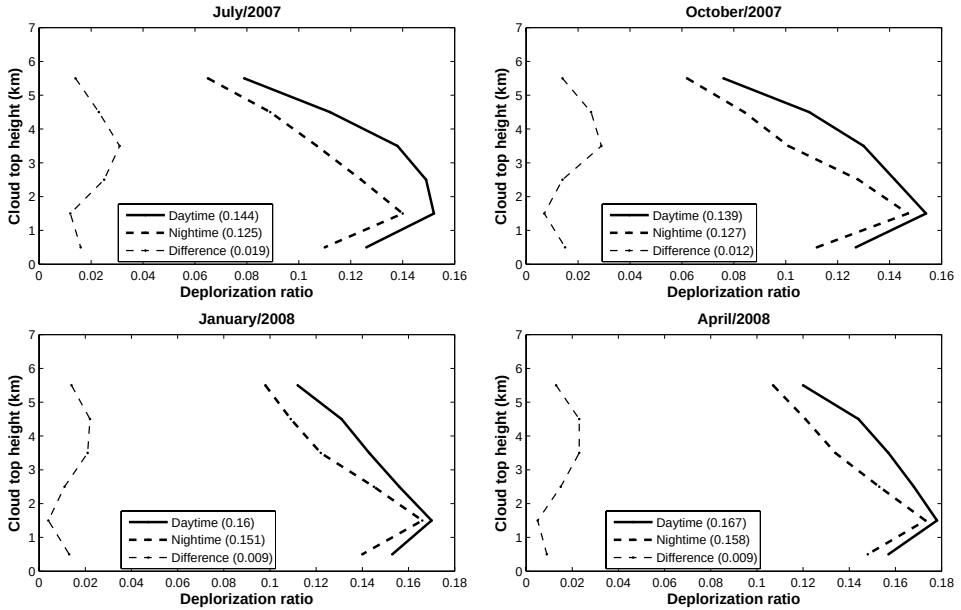

Fig. 8. The height dependency of global mean depolarization ratio for all level water clouds. The solid lines are for daytime, thicker dashed lines are for nighttime, thinner dashed lines are for the difference between day and nighttime. The values in the brackets are the global mean depolarization ratio for all water clouds.

ACPD
10, 28151–28181, 2010